Origin of Surface Canting within Fe_{3}O_{4} Nanoparticles

K. L. Krycka, J. A. Borchers, R. A. Booth, Y. Ijiri, K. Hasz, J. J. Rhyne, and S. A. Majetich

Phys. Rev. Lett. **113**, 147203 — Published 2 October 2014

DOI: 10.1103/PhysRevLett.113.147203

Origin of Surface Canting Within Fe_3O_4 Nanoparticles

K. L. Krycka and J. A. Borchers
*NIST Center for Neutron Research, Gaithersburg, MD, USA 20899**

R. A. Booth and S. A. Majetich
Carnegie Mellon University, Pittsburgh, PA, USA 15213

Y. Ijiri and K. Hasz
Oberlin College, Oberlin, OH, USA 44074

J. J. Rhyne
U.S. Department of Energy, Washington, D.C., USA 20585
(Dated: September 3, 2014)

The nature of near-surface spin canting within Fe_3O_4 nanoparticles is highly debated. Here we develop a neutron scattering asymmetry analysis which quantifies the canting angle to between 23^o and 42^o at 1.2 T. Simultaneously, an energy-balance model is presented which reproduces the experimentally observed evolution of shell thickness and canting angle between 10 K and 300 K. The model is based on the concept of T_d site reorientation and indicates that surface canting involves competition between Zeeman, exchange, magnetocrystalline anisotropy, and dipolar energies.

PACS numbers: 75.25.-j

Magnetite (Fe_3O_4) nanoparticles (NPs), attractive for their bio-compatibility and high Curie temperature [1], are important for biomedical technologies such as enhanced MRI contrast imaging, hyperthermia cancer treatment, and tagging. Almost universally Fe_3O_4 NPs display a reduced saturation magnetization (m_S) compared with bulk Fe_3O_4, which is exacerbated for decreased NP size and suggestive of a surface-related mechanism. Theoretical models indicate that sufficient surface anisotropy could induce a configuration of surface spins pointing radially outward [2–4] that reduces m_S. Surface disordering has also been widely proposed [5–8], yet recent studies indicate that capping with organic solvents such as oleic acid [9–11] or IGEPAL® CO-520 [12] can largely preserve the surface magnetization. Mössbauer spectroscopy and x-ray magnetic circular dichroism experiments [12–14] suggest that spin reorientation may occur in which the tetrahedral and octahedral Fe surface spins realign relative to one another, canting the NP surface. Small-angle neutron scattering (SANS) has shown that close-packed Fe_3O_4 NPs exhibit pronounced core|canted-shell morphology in an applied magnetic field, $\vec{H}$, of 1.2 T at 160 K to 320 K, but not at 10 K or in a remanent field [15].

This article develops a novel analysis of *2D* neutron angular asymmetry data combined with traditional magnetometry in order to obtain a quantitative vector magnetization profile of the canted shell. With this new insight, an energetically balanced model is constructed to explain this unusual core|shell morphology. Although the component of magnetization parallel to the applied field is found to be smaller in NPs than in bulk Fe_3O_4, the polarized neutron data reveal that the canted, local surface moments are equal to or enhanced compared with the NP interior, potentially exceeding bulk moments.

To minimize structural disorder, monodispersed Fe_3O_4 NPs prepared by high temperature chemical methods [16] are investigated. Transmission electron microscopy images yield a particle diameter distribution of 8.4 nm ± 1.3 nm; SANS data which are more sensitive to the larger particles fit well to a spherical NP form factor of 9.0 nm ± 0.2 nm [15]. The NPs are self-assembled into face-centered cubic (FCC) superlattices of unit length 13.6 nm [17] with long-range order approaching the micron level (*i.e.* NP crystals). Prior to crystallization, the NPs are washed to remove all but a thin capping layer of oleic acid. The magnetization (m) of the NPs is characterized using magnetometery and Polarization Analyzed SANS (PASANS), which measures the Fourier transform of the magnetic distribution across each NP ($|M|^2$) with vectorial sensitivity [18–24]. Fig. 1a provides a schematic of the PASANS set-up. m is expressed in the orthogonal components of $m_{\parallel\vec{H}}$ and $m_{\perp\vec{H}}$.

Magnetometry indicates that field-cooled NP $m_{\parallel\vec{H}}$ decreases (15 ± 3) % faster than bulk Fe_3O_4 from 10 K to 300 K [25]. If this decrease of $m_{\parallel\vec{H}}$ with increasing temperature was entirely due to changes within the shell region (m_{shell}) and m from within the core (m_{core}) was equal to that of bulk Fe_3O_4 ($m_{bulk} = m_{core}$), then $0.8 \leq \frac{m_{shell\parallel\vec{H}}}{m_{core}}$ sets the lower limit for $m_{shell\parallel\vec{H}}$ [25], in agreement with [9]. However, size-induced thermal fluctuations [26] likely also contribute to the observed temperature dependence, affecting m_{core} and m_{shell} alike. To ascertain the purely thermal reduction of NP m, we note that at 0.005 T (remanence) the NPs do not form canted shells, but instead exhibit uniform m across their interiors with semi-random orientation to neighboring NPs [15]. Based on the remanent field data [25], the thermal reduction ratio of $\frac{m_{NP\ at\ 300\ K,\ 0.005\ T}}{m_{NP\ at\ 200\ K,\ 0.005\ T}} = 0.87 \pm 0.02$. Compared to the canted-shell morphology at 1.2 T where $\frac{m_{NP\parallel\vec{H}\ at\ 300\ K,\ 1.2\ T}}{m_{NP\parallel\vec{H}\ at\ 200\ K,\ 1.2\ T}} = 0.90 \pm 0.01$ (SQUID) and 0.90 ± 0.03 (PASANS), we find that if the size-dependent thermal excitations affect m_{core} and m_{shell} equally, then $1.0 \leq \frac{m_{shell\parallel\vec{H}}}{m_{core}} \leq 1.5$ [25], suggesting that m_{shell} is preserved or even enhanced relative to m_{core}.

The canting angle of the shell can be determined through angular analysis of the *2D* PASANS patterns. Specifically, the scattered intensity that involves flipping of the neutron's spin (spin-flip scattering), $I_{SF}(\vec{Q})$, is given by [27]

$$I_{SF}(\vec{Q}) = |M_{\parallel\vec{H}}(\vec{Q})|^2 sin^2(\theta)cos^2(\theta) + |M_{\perp\vec{H}}(\vec{Q})|^2(1 + cos^4(\theta)) - \underbrace{2|M_{\parallel\vec{H}}(\vec{Q})||M_{\perp\vec{H}}(\vec{Q})|sin(\theta)cos^3(\theta)\overline{cos}(\delta\phi)}_{cross-term} \quad (1)$$

where θ is the angle between the scattering vector, Q, and the positive x-axis $\parallel \vec{H}$ (Fig. 1(a)). $\overline{cos}(\delta\phi)$ is the phase difference between $|M_{\parallel\vec{H}}(\vec{Q})|$ and $|M_{\perp\vec{H}}(\vec{Q})|$ which tends toward zero if the two are uncorrelated and unity if they are correlated [27]. In remanence $\overline{cos}(\delta\phi) = 0$ such that I_{SF} at $\theta = 0^o$ and 90^o simplifies to 2 and 1 times $|M_{\perp\vec{H}}(\vec{Q})|^2$ [23], as expected. At 1.2 T, however, this factor is remarkably reduced to 1.25 ± 0.12 at 200 K and at 300 K, Fig. 1(b,c). This is determined by taking sector slices of $\pm 10^o$ about the horizontal ($\theta = 0^o$) and vertical ($\theta = 90^o$) axes, Fig. 1(a), and dividing them as shown with red rectangles in Fig. 1(b,c). The horizontal:vertical suppression can be explained by a correlated ferrimagnetic core and a canted shell within the same NP ($\overline{cos}(\delta\phi) = 1$ at 1.2 T) giving rise to the negative cross-term [28] of Eq. 1. For a given $\frac{m_{shell\parallel\vec{H}}}{m_{core}}$, a unique $\frac{m_{shell\perp\vec{H}}}{m_{core}}$ value is determined by fitting the spin-flip horizontal:vertical ratio with a core|shell model [29] of shell thickness 1.0 nm ± 0.2 nm at 200 K, 1.2 T and 1.5 nm ± 0.2 nm at 300 K, 1.2 T combined with Eq. 1. Table I lists the corresponding range of fits at 200 K. The fifth row

of Table I, for example, produces the simulated scattering and horizontal/vertical ratio shown in blue and pink lines in Fig. 1(b,c) which agrees well with the data shown in black circles and red squares, respectively. The simulated high-Q portion can be better matched to the data by increasing m_{shell} relative to m_{core} while also lowering the net shell canting angle, $\epsilon = tan^{-1}\left(\frac{m_{shell\perp\vec{H}}}{m_{shell\parallel\vec{H}}}\right)$, Table I. The family of solutions consistent with the spin-flip suppression suggests a 1.2 T spin canting of $\epsilon = 27^o$ to 42^o at 200 K and $\epsilon = 23^o$ to 31^o at 300 K.

As a guide, bulk Fe_3O_4 is a cubic inverse spinel that contains Fe^{3+} tetrahedral (T_d^{3+} of 5 μ_B), Fe^{2+} octahedral (O_h^{2+} of 4 μ_B), and Fe^{3+} octahedral (O_h^{3+} of 5 μ_B) ions per formula unit ($f.u.$) $\equiv$ (0.42 nm)^3. The O_h sites align nearly anti-parallel to the T_d sites *via* indirect exchange through mediating O^{2-} ions [30], resulting in an uncompensated bulk m_S of 3.8 $\times 10^{-23}$ $JT^{-1}f.u.^{-1}$ (4.10 $\mu_B f.u.^{-1}$ = 2.37 x$10^{-4}eV f.u.^{-1}$). NP surface truncation may disrupt exchange coupling, allowing tilting between the T_d and O_h sites to develop [12–14] and resulting in a *local increase in m* (Table I). Yet, widespread T_d-O_h canting is energetically costly. Additionally, if $\frac{m_{shell\parallel\vec{H}}}{m_{core}} < 1$ (Table I, entries 1-2), then for $\vec{H} > 0$ the Zeeman energy increases unfavorably as well. To compensate, there could exist an anisotropy (K_V) energy savings associated with canting given that the NPs are fixed in place by oleic acid bonds such that their preferred (111) magnetocrystalline axes are randomly oriented with respect to $\vec{H}$ [25]. Alternatively, if $\frac{m_{shell\parallel\vec{H}}}{m_{core}} > 1$ (Table I, entries 4-8), then the exchange cost of canting may be offset by the Zeeman savings.

Let us first examine a simple model of uniform canting where $T_{d\ tilt} = O_{h\ tilt}$ (Table I, entry 1) driven by NP-enhanced anisotropy, where K_V of bulk Fe_3O_4 is 1.35 $\times 10^4 J\ m^{-3}$ ($6.24 \times 10^{-6} eV f.u.^{-1}$). In NP form the surface and magnetocrystalline anisotropy have been observed to couple such that the effective anisotropy can be enhanced by factors (κ) of 1.6 [31], 3.3 [32], or even ≈ 10 [33]. Neglecting the small dipolar coupling and the large exchange energy costs for now, we note that the maximum anisotropy-driven energy savings per $f.u.$ (defined as the negative minimum in total energy) associated with shell formation is

$$\Delta E_{shell\ f.u.^{-1}} = \overbrace{2.37 \times 10^{-4}\ eV\ T^{-1}(1 - cos(\epsilon))\ 1.2\ T}^{Zeeman\ Cost} - \overbrace{6.24 \times 10^{-6}\ eV(cos(55^o - \epsilon) - cos(55^o))\ \kappa}^{Effective\ Anisotropy\ Savings} \tag{2}$$

where ϵ is the net shell canting angle and 55^o is the maximum angle between $\vec{H}$ and the nearest (111) anisotropy axis. For $\kappa = 1$ (no anisotropy enhancement) the lowest-energy results from $\epsilon = 0^o$ (no canting); $\kappa = 10$ results in only $\epsilon = 9^o$; $\kappa = 90$ is needed for $\epsilon = 37^o$, consistent with entry 1 of Table I. Thus, without an extraordinary increase in NP anisotropy, this mechanism alone is unlikely to account for the canted shell formation.

Now, let us consider the second possibility that T_d canting [12, 13] negates the exchange cost by locally increasing m (resulting in Zeeman energy savings). As depicted in Fig. 2(a), the NPs are modeled as discrete cubic $f.u.$'s assembled to approximate 9 nm spheres, which are further close-packed into a FCC array of unit lattice length 13.6 nm to replicate experimental conditions. Temperature dependence is intrinsically built into $m \propto \beta$, where β is the ratio of NP m to m_S of bulk Fe_3O_4. At 1.2 T β varies from 0.88 at 10 K, 0.80 at 160 K, 0.75 at 200 K, 0.65 at 300 K, and 0.60 at 320 K [25]. Summing over $f.u.$ indices, i, we find that the Zeeman energy per NP is

$$E_{zeeman} = -\sum_{i\ within\ NP} \vec{m}_i \cdot \vec{H}. \tag{3}$$

Internal dipolar energy is nearly negligible, but inter-particle dipolar energy is more substantial and is calculated over the 18 closest nearest-neighbors within the lattice of NPs (with NP locations indicated by i and j) assuming that each NP is magnetically equivalent:

$$E_{dipole} = \sum_i \sum_{j \neq i} \frac{\mu_o\,(\vec{m}_i \cdot \vec{m}_j - 3(\vec{m}_i \cdot \vec{r}_{ij})(\vec{m}_j \cdot \vec{r}_{ij}))}{4\pi \|\vec{r}_{ij}^{\,3}\|} \tag{4}$$

The average NP crystalline anisotropy constant (K_V) is set to $\kappa = 4$ times bulk Fe_3O_4 (0.13 eV per NP) based on [31–33] yielding per NP:

$$E_{anisotropy} = -[cos^2(\theta_{ave} - T_{d\ tilt}) \cdot \overbrace{\frac{R^3 - (R-t)^3}{R^3}}^{shell\ fraction} + cos^2(\theta_{ave}) \cdot \overbrace{\frac{(R-t)^3}{R^3}}^{core\ fraction}\ ] \cdot \frac{0.13\ eV}{NP} \tag{5}$$

where $\theta_{ave} = 27.5^o$ is the average angle of the preferred (111) or equivalent crystalline axis within each NP with respect to $\vec{H}$, $R = 4.5$ nm is the NP radius, and t is the canted shell thickness. The exchange energy per NP is:

$$E_{exchange} = \frac{-J_{exch}}{f.u.} \cdot \beta \cdot (1 - cos(T_{d\ tilt})) \cdot \sum_{i=1}^{R/\delta(t)} \omega \cdot \underbrace{\frac{4\pi}{3} \frac{(R - i\delta(t))^3 - (R - (i-1)\delta(t))^3}{f.u.^3}}_{f.u.'s\ per\ annular\ slice} \tag{6}$$

where $T_{d\ tilt}$ is the average tilt of the T_d Fe sites with respect to the applied field, Fig. 2(a), and $\delta(t)$ discretizes the NP into annular rings 0.05 nm thick. $T_{d\ tilt}$ is varied in increments of 5^o and t is varied in increments of 0.1 nm. The correction, $\omega = \frac{R}{3(R-i\delta(t))}$ if $i\delta(t) \leq 3$ nm and $\omega = 1.0$ if $i\delta(t) \geq 3$ nm, accounts for the decrease in the number of surrounding nearest neighbor $f.u.$'s, reaching 0.33 at the NP edge. J_{exch} is the only fit parameter, and the model is consistent with the observed shell thicknesses at J_{exch} of 1.80 meV/$f.u.$ to 1.90 meV/$f.u.$ [25]. This value is reasonable given that T_d-O_h bonds in a perfect crystal range from 2.0 meV to 2.9 meV [30, 34].

Simulations at 1.2 T are shown in Fig. 2(b-f) for $J_{exch} = 1.85$ meV/$f.u.$ The energetically selected configurations are $t = 1.6$ nm with $T_{d\ tilt} = 15^o$ at 300 K (and also at 320 K, not shown), $t = 1.2$ nm with $T_{d\ tilt} = 20^o$ at 200 K, and $t = 0.9$ nm with $T_{d\ tilt} = 30^o$ at 160 K. These simulated t's are all consistent with experiment [15]. Including the uncertainty of R ($\pm$ 0.1 nm) or of J_{exch} ($\pm$ 0.05 meV) slightly broadens the $T_{d\ tilt}$ range to between 15^o and 20^o ($\epsilon = 17^o$ to 22^o) at 300 K, 1.2 T and $T_{d\ tilt} = 15^o$ to 30^o ($\epsilon = 17^o$ to 28^o) at 200 K, 1.2 T [25], on the low end of agreement with the PASANS-determined spin canting discussed above. At 10 K the energy minimum tends toward a mixture of shells at $t = 0.3$ nm, 0.7 nm, and 0.9 nm with $T_{d\ tilt}$ between 50^o and 85^o. The mixture of multiple shell thicknesses would blur out the characteristic spin-flip dip used to identify a core|shell morphology, also consistent with experimental observation [15]. We note that although 10 K is below a possible Verwey transition, the exchange constant should not change [34]. Finally, at 300 K, 0.005 T the minimum energy spans a wide range of nearly equivalent t's with a preferred $T_{d\ tilt} = 5^o$, which is sufficiently shallow that canting would be difficult to detect experimentally for a system of NPs with random magnetic core alignment [15].

Recall that temperature is encompassed by β, where dipole energy $\propto \beta^2$, Zeeman and exchange are $\propto \beta$, and anisotropy is independent of β. This means that as temperature is increased, the constant contribution of anisotropy (favoring thicker shells) increases *relative* to the other terms. This explains the trend toward thicker shells at higher temperature. Yet, the exchange cost progressively increases as the canted shell thickens and the number of nearest Fe neighbors approaches the bulk Fe_3O_4 level. Thus, shell thickening is associated with a decrease in canting angle between 160 K and 300 K (Fig. 2(b-d)). We note that although the 10 K, 1.2 T simulation shows multiple minima of comparable energies (no well defined shell), the trend of thinner shells with increased canting angle is preserved compared with higher temperatures, Fig. 2(e).

To compare the relative energy contributions involved, Fig. 3(a) shows the 160 K, 1.2 T energy minima at $T_{d\ tilt} = 30^o$ as a function of t. As expected, the dominant energy terms are the Zeeman energy savings (thicker shell with increased tilt preferred) and the exchange energy cost (thinner shell with decreased tilt preferred). Yet, the presence of both the dipolar and anisotropy contributions modify the shell thickness, as indicated in Fig. 3(b).

In conclusion, a novel PASANS analysis of the $2D$ scattering asymmetry reveals the vectorial nature of magnetic canting within the near-surface shell region of Fe_3O_4 NPs, yielding a net shell canting angle between 23^o and 42^o. A model of Fe-site T_d tilting [12, 13] away from its nominal anti-$\parallel \vec{H}$ arrangement is proposed which reproduces (*i*) the measured scattering asymmetry, (*ii*) canted shell formation at high magnetic field, and (*iii*) the observed increase in canted shell thickness and decrease in canting angle with increasing temperature. While the input values of anisotropy, exchange, and magnetization variation near the surface may need to be refined, this model clearly demonstrates that the interplay between exchange, Zeeman, inter-particle dipolar coupling, and anisotropy energies is capable of inducing surface spin canting. Both the model and experimental data indicate that application of high fields increases the local m within the canted region compared to its non-canted state, driven in part by Zeeman energy. Additionally, a model which selects for canted shells of finite thickness requires that the near-surface exchange coupling decrease toward the NP surface, explainable as a decrease in nearest-neighbor Fe-sites. We thus provide a physical, energy-based explanation to the long-standing question of reduced magnetization in magnetite NPs and expect that with appropriate adjustment of anisotropy and exchange constants, the model could be applied successfully to other nanostructured systems.

This work utilized facilities supported in part by National Science Foundation grants DMR-0944772 and DMR-1104489 and Department of Energy grant DE-FG02-08ER46481. We thank W.C. Chen and S.M. Watson for their assistance with the polarized ^{3}He spin filters and P. Kienzle for his discussions regarding locating energy minima.

* kathryn.krycka@nist.gov

[1] J. Wang, W. Wu, F. Zhao, and G. Zhao, *Appl. Phys. Lett.* **98**, 083107 (2011).
[2] L. Berger, Y. Labaye, M. Tamine, and J. M. D. Coey, *Phys. Rev. B.* **77**, 104431 (2008).
[3] J. Mazo-Zuluaga, J. Restrepo, F. Muõz, and J. Mejía-López, *J. Appl. Phys.* **105**, 123907 (2009).
[4] Y. Hu and A. Du, *J. Nanosci. Nanotechnol.* **9**, 5829 (2009).
[5] P. Dutta, S. Pal, M. S. Seehra, N. Shah, and G. P. Huffman, *J. Appl. Phys.* **105**, 07B501 (2009).

[6] J. Curiale, M. Granada, H. E. Troiani, R. D. Sanchez, A. G. Leyva, P. Levy, and K. Samwer, *Appl. Phys. Lett.* **95**, 043106 (2009).

[7] A. Kovács, K. Sato, V. K. Lazarov, P. L. Galindo, T. J. Konno, and Y. Hirotsu, *Phys. Rev. Lett.* **103**, 115703 (2009).

[8] C. Westman, S. Jang, C. Kim, S. He, G. Harmon, N. Miller, B. Graves, N. Poudyal, R. Sabirianov, H. Zeng, M. DeMarco, and J. P. Liu, *J. Phys. D: Appl. Phys.* **41**, 225003 (2008).

[9] J. Salafranca, J. Gazquez, N. Pérez, A. Labarta, S. T. Pantelides, S. J. Pennycook, X. Batlle, and M. Varela, *Nano Lett.* **12**, 2499 (2012).

[10] A. G. Roca, D. Niznansky, J. Poltierova-Vejpravova, B. Bittova, M. A. Gonzalez-Fernandez, C. J. Serna, and M. P. Morales, *J. Appl. Phys.* **105**, 114309 (2009).

[11] P. Guardia, B. Batlle-Brugal, A. G. Rocab, O. Iglesias, M. P. Morales, C. J. Serna, A. Labarta, and X. Batlle, *J. Magn. Magn. Mater.* **316**, e756 (2007).

[12] M. Darbandi, F. Stromberg, J. Landers, N. Reckers, B. Sanyal, W. Keune, and H. Wende, *J. Phys. D: Appl. Phys.* **45**, 195001 (2012).

[13] S. Brice-Profeta, M. A. Arrio, E. Tronc, N. Menguy, I. Letard, C. Cartier dit Moulinc, M. Noguès, C. Chanéac, J. P. Jolivet, and Ph. Sainctavit, *J. Magn. Mag. Mater.* **288**, 354 (2005).

[14] J. M. D. Coey, *Phy. Rev. Lett.* **27**, 1140 (1971).

[15] K. L. Krycka, R. A. Booth, C. R. Hogg, Y. Ijiri, J. A. Borchers, W. C. Chen, S. M. Watson, M. Laver, T. R. Gentile, L. R. Dedon, S. Harris, J. J. Rhyne, and S. A. Majetich, *Phys. Rev. Lett.* **104**, 207203 (2010).

[16] S. Sun, H. Zeng, D. B. Robinson, S. Raoux, P. M. Rice, S. X. Wang, and G. Li, *J. Am. Chem. Soc.* **126**, 273 (2004).

[17] D. F. Farrell, Y. Ijiri, C. V. Kelly, J. A. Borchers, J. J. Rhyne, Y. Ding, S. A. Majetich, *J. Magn. Magn. Mater.* **303**, 318 (2006).

[18] R. M. Moon, T. Riste, and W. C. Koehler, *Phys. Rev.*, **181**, 920 (1969).

[19] O. Schärpf and H. Capellmann, *Physica Status Solidi A* **135**, 359 (1993).

[20] A. Wiedenmann, *Physica B* **1**, 246 (2005).

[21] J. F. Löffler, H. B. Braun, W. Wagner, G. Kostorz, and A. Wiedenmann, *Phys. Rev. B* **71**, 134410 (2005).

[22] A. Michels and J. Weissmüller, *Rep. Prog. Phys.* **71**, 066501 (2008).

[23] K. L. Krycka, R. Booth, J. A. Borchers, W. C. Chen, C. Conlon, T. R. Gentile, C. Hogg, Y. Ijiri, M. Laver, B. B. Maranville, S. A. Majetich, J. J. Rhyne, S. M. Watson, *Physica B*, **404B**, 2561 (2009).

[24] W. Schweika, *J. Phys.: Conf. Ser.* **211**, 012026 (2010).

[25] See supplementary material at http://link.aps.org/supplemental/xx.xxxx/PhysRevLett.xxx.xxxxxx.

[26] S. Mørup and B. R. Hansen, *Phys. Rev. B* **72**, 024418 (2005).

[27] K. Krycka, J. Borchers, Y. Ijiri, R. Booth, and S. Majetich, *J. Appl. Cryst.* **45**, 554 (2012).

[28] A. Michels, S. Erokhinb, D. Berkovb, and N. Gorn, *J. Magn. Mag. Mater.* **350**, 55 (2014).

[29] S. R. Kline, *J Appl. Cryst.* **39**, 895 (2006).

[30] M. Uhl, and B. A. Siberchicot, *J. Phys.: Condens. Matter* **7**, 42274237 (1995).

[31] E. Lima Jr., A. L. Brandl, A. D. Arelaro, and G. F. Goya, *J. Appl. Phys.* **99**, 083908 (2006).

[32] G. Salazar-Alvarez, Royal Institute of Technology (KTH), Sweden, Ph.D. Thesis, Synthesis, Characterisation and Applications of Iron Oxide Nanoparticles, 2004.

[33] D. Caruntu, G. Caruntu, and C. J. O'Connor, *J. Phys. D.: Appl. Phys.* **40**, 5801 (2007).

[34] H. A. Alperin, O. Steinsvoll, R. Nathans, and G. Shirane, *Phys. Rev.* **154**, 508 (1967).

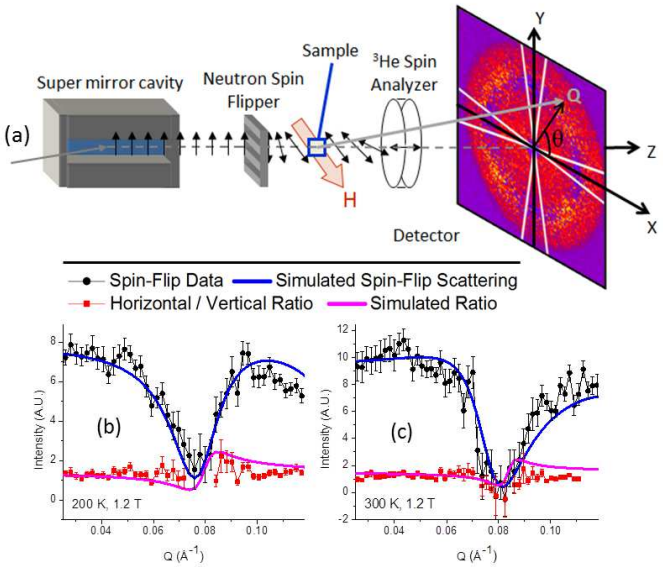

FIG. 1. (a) PASANS set-up with polarizing neutron spin optics. White lines indicate regions of horizontal and vertical sector slices. At 1.2 T, 200 K (b) and 300 K (c) spin-flip data are shown in black circles, while simulated data based on Table I, entry 5 are shown with blue lines. The horizontal:vertical ratios, red triangles, are < 2 due to the negative cross-term in Eq. 1. Points around 0.075 $\AA^{-1}$ which approach zero have been removed from the ratio, and the 300 K ratio is limited to 0.11 $\AA^{-1}$ due to limited vertical angular acceptance. Simulated ratios (Table I, entry 5) are shown with pink lines. Error bars here and in the text indicate one standard deviation.

TABLE I. Choice of $\frac{m_{shell\|\vec{H}}}{m_{core}}$ plus horizontal:vertical ratio, Fig. 2(b), produces a unique $\frac{m_{shell\perp\vec{H}}}{m_{core}}$ value at 200 K, 1.2 T. Corresponding T_d and O_h angles are calculated [25]. Note that for $m_{shell} \geq m_{core}$ most of the canting is taken up by tilting of the T_d site. A more general shell canting angle, ϵ, is also calculated and can be associated with a T_d-only tilt (for $\epsilon \leq 33^o$) if we assume that the intrinsic (uncanted) values of $|m_{core}|$ and $|m_{shell}|$ regions are equivalent. Ranges given in brackets are the result of varying shell thickness within uncertainty [25].

Entry	$\frac{m_{shell\|\vec{H}}}{m_{core}}$	$\frac{m_{shell\perp\vec{H}}}{m_{core}}$	T_d, O_h tilts	Shell Cant (ϵ)	T_d-only tilt
1	0.80	0.60 (0.52-0.71)	37^o, 37^o	37^o (33^o-42^o)	NA
2	0.90	0.63 (0.56-0.75)	1^o, 17^o	35^o (32^o-40^o)	NA
3	1.0	0.66 (0.59-0.78)	13^o, -10^o	33^o (30^o-38^o)	46^o
4	1.1	0.70 (0.62-0.82)	25^o, -4^o	33^o (30^o-37^o)	46^o
5	1.2	0.74 (0.66-0.85)	33^o, -2^o	32^o (29^o-35^o)	40^o
6	1.3	0.77 (0.70-0.89)	41^o, 1^o	31^o (28^o-34^o)	37^o
7	1.4	0.81 (0.73-0.92)	48^o, 3^o	30^o (28^o-33^o)	35^o
8	1.5	0.85 (0.78-0.97)	54^o, 4^o	30^o (27^o-33^o)	35^o

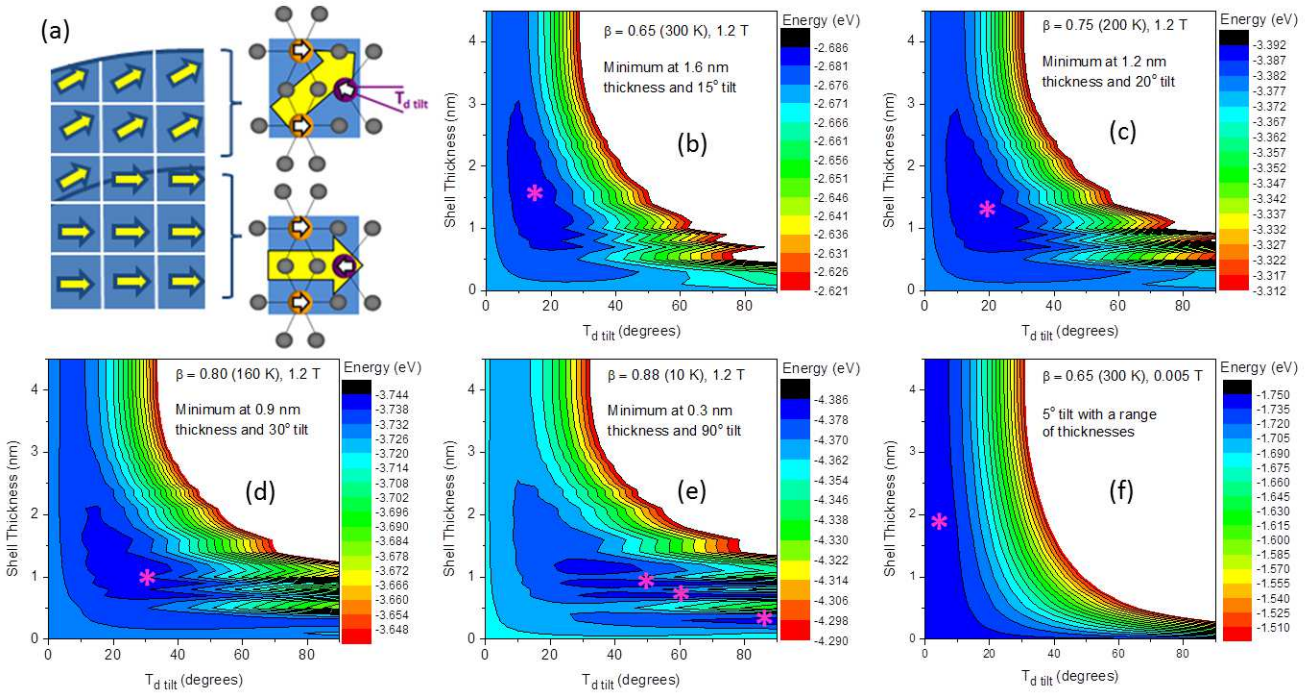

FIG. 2. (a) Near-edge section of a core|canted-shell model broken into cubic formula units of length 0.42 nm. Insets show constituent T_d (purple) and O_h (orange) Fe-sites; yellow arrows indicate the net local moments moments of these constituent Fe spins. Simulated energy landscapes as a function of t and $T_{d\ tilt}$ at 1.2 T are shown for 300 K (b), 200 K (c), 160 K (d), and 10 K (e). Remanence at 300 K is shown in (f). Pink stars indicate global minima; white space indicates areas of high energy.

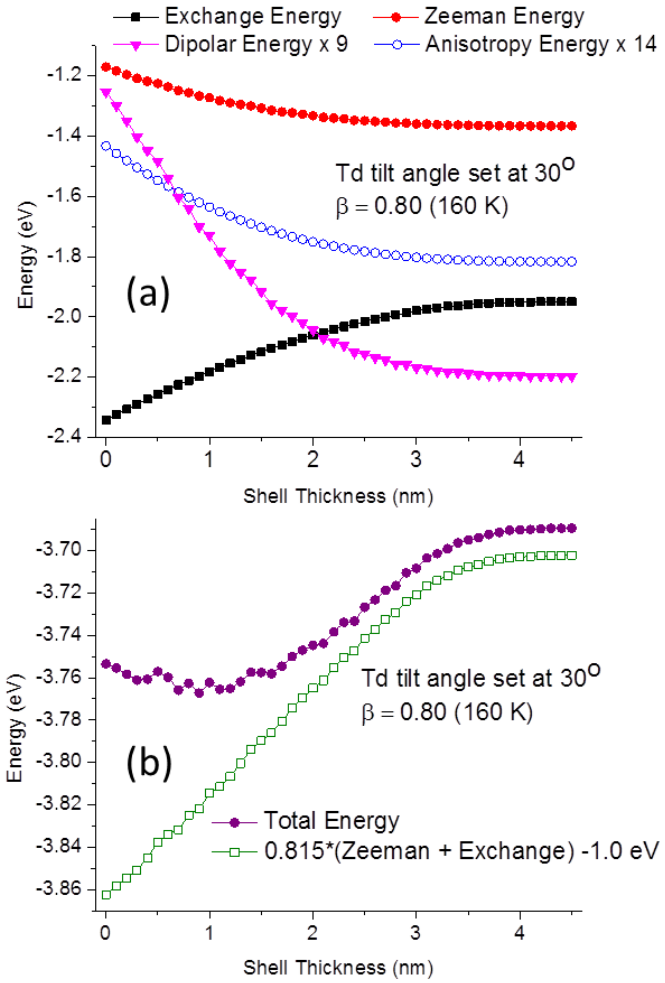

FIG. 3. (a) Energy contributions at 160 K, 1.2 T as a function of shell thickness (t) are dominated by Zeeman and exchange energies. (b) The sum of these energies produces a minimum at $t = 0.9$ nm (purple circles), although without the inclusion of both dipole and anisotropy contributions the minimum would shift toward $t = 0$ nm (green open squares).